

Reading 7: Medical Imaging

For many years, photographic film was the principal means for storing medical images. Computers have provided a new means for storing, processing, transferring, and displaying images. First used for computerized tomography, computers and digital image processing have engendered a revolution in the way medical images are produced and manipulated. Now it is possible to acquire data, perform mathematical operations to produce images, emphasize details or differences of images, and store and retrieve images from remote sites, all without film. Telephone lines and other communication means such as the Internet with common standards of image communication make possible the near instant display of the information needed for diagnosis.

Photographic, x-ray, ultrasonic, radionuclide, television, and other imaging systems can be thought of as cameras. All camera images are limited by resolution, amplitude scale, and noise content. The photographic image can be enlarged until it becomes quite grainy, and this graininess is the bound on both resolution and noise. The x-ray image is resolution limited by the dimensions of the x-ray source and noise limited by the beam intensity. The ultrasound image is limited by the angular resolution of the transducer and its ability to separate true signals from false signals and noise.

An image can be studied without regard to the camera that produced it. A camera can be considered a device that transfers an image from one surface to another. It can be defined as an aperture through which the signals related to all elements of the original image must pass to appear in the final image. A camera—whether a television, x-ray, or other image-forming device—can be described in terms of its spatial-transfer function.

Radiography produced the first medical images of the inside of the body. X-ray photons are electromagnetic radiation, as are light photons. However, light photons have an energy of 2 to 4 eV and x-ray photons have an energy of 20 to 150 keV, about 10^4 times more energy than light photons. This higher energy makes x-ray photons more penetrating than light photons. Streams of x-ray photons can dissociate molecules by ionization and are thus called ionizing radiation. X rays damage the body in proportion to both the amount and rate of radiation as the body is normally in a constant state of damage and repair. Roentgen first observed x rays in 1895 as he experimented with a device that had a beam of electrons striking a metal target and he observed the fluorescence of some crystals several meters away.

MEASUREMENT OF X RAYS

The Roentgen is defined as the incident radiation causing a conducted charge of 2.58×10^{-4} C/kg in air, a definition which accounts for changes of temperature and pressure. The original unit of absorbed dose is the *rad*, defined as an absorbed energy of 10^{-2} J/kg. Because about 33.7 eV are needed to form one ion pair in dry air, one R is the equivalent of 0.87 r. Not all photon energies of ionizing radiation incident to a patient have the same effect: Beams of more energetic photons can produce greater tissue damage for the same measured radiation. To account for different biological effects, the absorbed dose in rad is multiplied by a “biological effect” factor of about 1.0 in the low energy range (up to 150 keV/photon) and about 4.0 (in the 4 MeV range) and the resulting absorbed dose is expressed in rem (radiation effect in man).

The modern unit of radiation replacing the rad is the *gray* (Gy), defined as 1 J/kg in dry air and the modern unit of exposure is the *sievert* (Sv), the number of grays times the biological effect factor. Both units are 100 times greater than their older equivalents, the rad and the rem.

BACKGROUND RADIATION

We live in a world of background radiation, cosmic radiation, including that of the sun, and the natural radioactivity of the earth caused by disintegration of the heavier elements. A product of these disintegrations, *radon*, may seep through rock formations and invade the lower levels of our homes. Radon disintegration products may attach themselves to dust or smoke particles and find their way inside our bodies. The radiation of medical and dental x-ray machines, smoke detectors, package inspection machines, and other devices also affect the amount of background radiation. Like chlorine in water, very small amounts of radiation are not harmful, and may be beneficial. Large

amounts can harm tissue, and this fact has been used to devise schemes to destroy cancerous tissue.

The natural background radiation ranges from 5×10^{-3} to 2×10^{-2} Sv/year. A few areas of the world have levels more than ten times higher. There is no statistically significant increase in deaths due to cancer for those living in areas of higher background. For people working with radiation, safe levels of occupational exposure are limited to 5×10^{-2} Sv/year. Nonoccupational exposure is limited to 5×10^{-3} Sv/year, a little above the background level. While ionizing radiation damages tissue, the slow rate of background exposure permits the body to repair the damage. A single whole body exposure of 6 Sv is the *mean lethal dose* (MLD); half of the people so exposed will die within a month. Yet, a lifetime exposure of 10 Sv appears harmless in that population exposures at this level will increase the incidence of cancer less than 1%. Not all tissue types are equally sensitive to the effects of exposure to ionizing radiation. A fetus is particularly sensitive as are the lens of the eye, bone marrow, the breast, and lung tissue. As a result, techniques have been developed to obtain radiographs with exposures as *low as reasonably achievable*, the ALARA principle.

GENERATION OF X RAYS

A simple x-ray system consists of a high voltage generator, an x-ray tube, a collimator, the object or patient, an intensifying screen, and the film (see Figure 12.5). A simple x-ray generator has a line circuit breaker, a variable autotransformer, an exposure timer and contactor, a step-up transformer and rectifier, and a filament control for the tube. Medical exposures are of the order

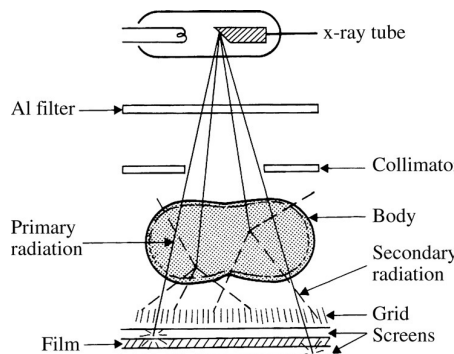


Figure 12.5 The x-ray tube generates x rays that are restricted by the aperture in the collimator. The Al filter removes low-energy x rays that would not penetrate the body. Scattered secondary radiation is trapped by the grid, whereas primary radiation strikes the screen phosphor. The resulting light exposes the film.

12.7 COMPUTED TOMOGRAPHY

A conventional x-ray image is limited because it is generated by projection from the x-ray source through the object onto the film. If there are regions of small and large variations in electron density along the same beam path, then small variations cannot be detected. An example of this is the conventional chest radiograph where dense bony structures make it difficult to derive information about the less-dense-tissue information in the lung fields.

One way to minimize this obstruction of one structure by another is to expose radiographs from several directions. This may not be practical because of the higher exposure received by the patient. In recent years, however, technology has yielded new ways of extracting more information from each transmitted photon so that better information on electron density of objects may be determined to reveal otherwise-hidden structures through multidirectional exposures.

Computed tomography is the name given to the diagnostic imaging procedure in which anatomical information is *digitally reconstructed* from x-ray transmission data obtained by scanning an area from many directions in the same plane to visualize information in that plane. The ideas involved were originally developed for imaging the brain. The dynamic range of densities in the brain is only a few percent, but the brain is encased in a bony structure so dense that most of the x rays are absorbed by the bony structure. Imaging of the brain by conventional radiography is difficult even when contrast is enhanced by injection of contrast materials or air. In concept, CT solves the set of simultaneous equations involving thousands of attenuation coefficients, μ_{ij} , for each ij element over the dozens of directions ("projections") used. Along a line of a given direction, the total attenuation is related to the sum of the individual attenuation coefficients:

For a single element, $I = I_0 e^{-\mu x}$ or $\ln I/I_0 = -\mu x$. For a series of elements of equal thickness,

$$\ln I/I_0 = -\Delta x e - D x (\mu_1 + \mu_2 + \mu_3 + \mu_4 + \dots)$$

where I is the exit beam intensity, I_0 is the initial beam intensity, x is the layer thickness, Δx is the thickness of an element of constant size, μ is the attenuation coefficient, and μ_i is the absorption coefficient of a particular series element.

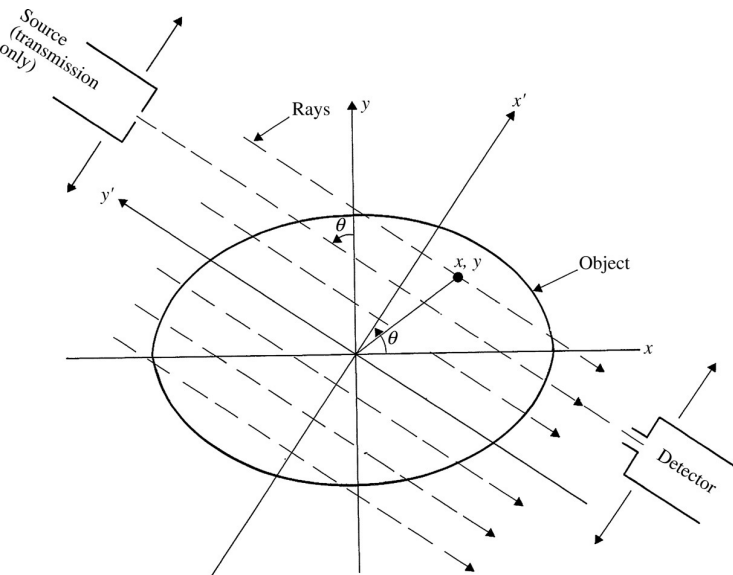


Figure 12.11 Basic coordinates and geometry for computed tomography The projection rays shown represent those measured at some angle θ . The source and detector pair is rotated together through a small angle, and a new set of rays measured. The process is repeated through a total angle of 180° . [From Brooks and Di Chiro (1975).]

Figure 12.11 is a schematic diagram of the scanning operation of the “first-generation” CT machines. A collimated beam of x rays is passed through the patient’s head in a direction transverse to the longitudinal axis. The emerging beam flux on the opposite side of the patient is constantly monitored in a scintillation detector. The x-ray source and detector move together, perpendicular to the beam direction, and roughly 160 distinct measurements of total attenuation of the x-ray beam are made at evenly spaced points along the scan path. The configuration of x-ray beam source and detector is then rotated through a small angle, usually 1° , and the procedure is repeated. The acquisition of absorption information by scanning is continued until an angle of 180° has been swept.

The procedure is called *tomography* (the Greek root *tomos* means to cut or to section) because only those structures lying in the narrow anatomical slice traversed by the beam are imaged. The tightly collimated beam results in imaging that is essentially scatter free and is efficient enough to make applying the procedure practical.

Fundamental to the procedure is the mathematical discovery that a two-dimensional function is determined by its *projections* in all directions. A sampling of projections at angles uniformly distributed about the origin can provide an approximate reconstruction of the function. How much detail

can be reconstructed is straightforwardly dependent on the number of angles sampled and the sampling coarseness at each angle. If beam absorption is measured at 160 distinct points along each scanning path and a 1° increment in angle is used, nearly 29,000 distinct pieces of x-ray absorption data are acquired. These are employed to reconstruct a two-dimensional map of x-ray absorption as a function of position, presented as a 160×160 matrix of uniform square-picture elements.

The reconstruction of images from the scanning data is performed by means of a small digital computer. The time required for reconstructing the picture is of the same order of magnitude as that for acquiring the data. Some of the mathematical reconstruction algorithms permit reconstruction to begin as soon as the first projection data come in. These algorithms clearly provide a considerable saving in time by allowing the mathematical reconstruction to take place during the scan operation.

The mathematical algorithms fall into two general classes, the iterative and the analytic. In the *iterative* methods, an initial guess about the two-dimensional pattern of x-ray absorption is made. The projection data predicted by this guess are then calculated, and these predictions are compared with the measured results. Discrepancies between the measured values and the model predictions are employed in a continuous iterative improvement of the model array.

Figure 12.12 shows the scheme by which the model projections are generated and by which the discrepancies between model and measurement are used to best improve the model at each iteration. Each reconstructed picture element is represented by an average attenuation coefficient μ_{ij} , where the subscripts i and j specify the position of the picture element in the image. The relative degree to which each element can remove x-ray flux from the ray at the k th beam position at scan angle θ is expressed by the four-label quantity $W_{ij}^{\theta k}$. These quantities are essentially determined by the geometrical overlap between the finite-width x-ray beam at scan position θk and the square-picture element at position ij . Clearly, the overwhelming majority of the more than 8×10^8 quantities $W_{ij}^{\theta k}$ are zero, because in most cases the ray θk does not pass through the element ij at all. The model array μ_{ij} determines the model projection data at each iteration according to

$$I^{\theta k} = I_0 \exp\left(-\sum_{ij} W_{ij}^{\theta k} \mu_{ij}\right) \quad (12.14)$$

$$P^{\theta k} = \ln\left(\frac{I_0}{I^{\theta k}}\right) = \sum_{ij} W_{ij}^{\theta k} \mu_{ij}$$

where I_0 is the constant intensity of the input beam and $I^{\theta k}$ is the intensity transmitted of position k at angle θ . The quantities $P^{\theta k}$, conventionally called the projection data for the position k at angle θ , are calculated in the manner shown in order that the observed measurements be converted into quantities that are simple linear combinations of the unknown quantities μ_{ij} .

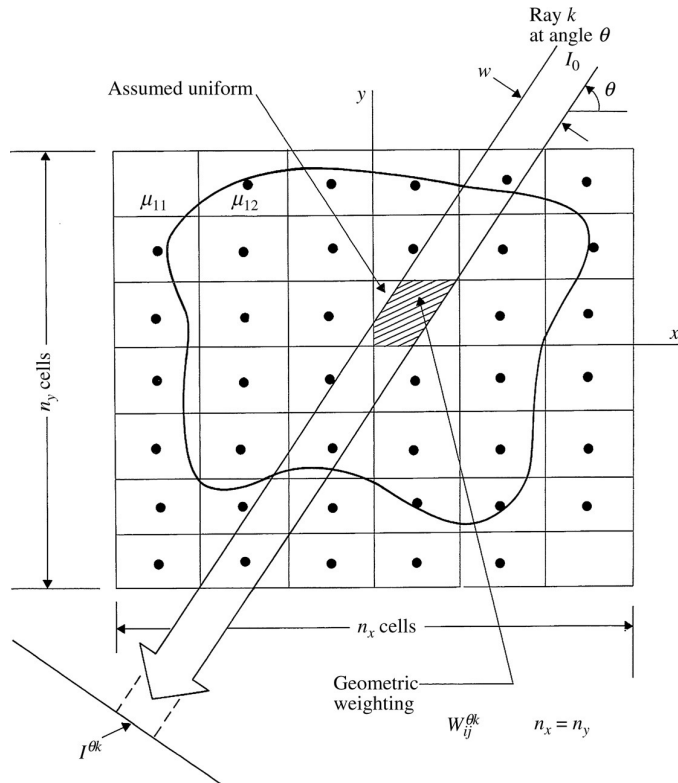


Figure 12.12 The basic parameters of computerized image reconstruction from projections. Shown are the picture element cells μ_{ij} , a typical projection ray $I^{θk}$, and their geometrical overlap $W_{ij}^{θk}$. [From Hall (1978).]

Just as the weights $W_{ij}^{θk}$ determine which picture elements are involved in the generation of the model projections, they also determine the manner in which the model array is changed at each iteration. In the simplest iterative reconstruction techniques, the discrepancy between the measured and model values of $P^{θk}$ is attributed equally to all the elements ij traversed by the ray $θk$, and each model-picture element is changed, according to the geometrical weights $W_{ij}^{θk}$, to make the model value and the measured value for the scan line under consideration come into agreement. In actual practice, many timesaving variations of this fundamental idea have been successfully tried. Regardless of the exact way in which the model array is modified, the rays $θk$ are cyclically iterated until the model values and the measurements of all ray projections are in adequate agreement.

Analytic methods differ from iterative methods in a very important way. In analytic methods, the image is reconstructed directly from the projection data without any recourse to comparison between the measured data and the

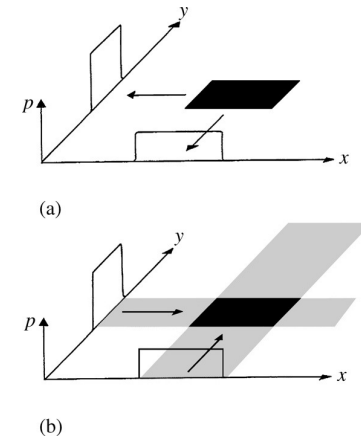


Figure 12.13 Back projection (a) Projections of this object in the two directions normal to the x and y axes are measured. (b) These projection data are projected back into the image plane. The area of intersection receives their summed intensities. It is apparent that the back-projected distribution is already a crude representation of the imaged object. [From Brooks and Di Chiro (1975).]

reconstructed model. Fundamental to analytic methods is the concept of *back projection*.

Figure 12.13 illustrates back projection for the case of projections at two angles separated by 90° . As shown, a back-projected image is made by projecting the scan data $P^{θk}$ back onto the image plane such that the projection value measured for a given ray is applied to all the points in the image plane that lie on that ray.

The total back-projected image is made by summing the contributions from all the scan angles $θ$. The summing is carried out by using the same geometrical weights defined in the preceding paragraph. The back-projected image is already a crude reconstruction of the imaged object. More important, the exact relationship between the back-projected image and the desired actual array of attenuation is well understood; the latter can be calculated from the former via Fourier analysis. The back-projected image is Fourier transformed into the frequency domain and filtered with a filter proportional to spatial frequency up to some frequency cutoff. The result is then transformed back into Cartesian coordinates.

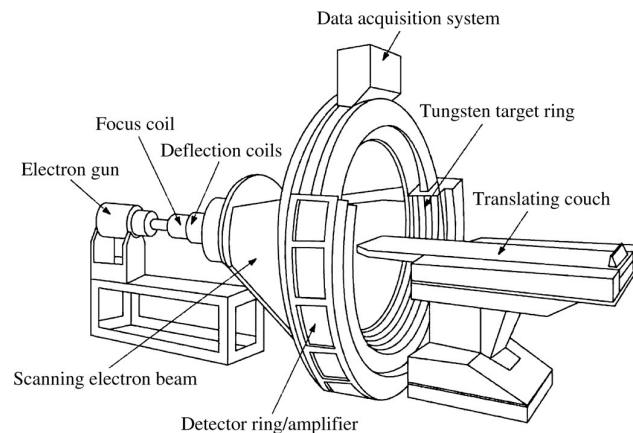


Figure 12.14 IMATRON electron beam CT system. (Courtesy of Doug Boyd, IMATRON Corp.)

The first-generation machines used a single pencil beam and a single detector in a translate-rotate scan. Each translation took about 5 s followed by a rotation of 1°, then 1 s delay for the machine to stop vibrating, followed by another translation of the x-ray tube and detector. To rotate over the full 180° took about 20 min. Because x-rays cannot be focused, the x-ray beam was limited to the dimensions of the detector by “coning,” using a leaded box in front of the x-ray tube with a hole scaled to the dimension of the detector.

The second generation used an array of 100 or more detectors spaced every 5 mm and the x-ray tube output shaped as a fan beam. The detectors and the x-ray tube rotated together, and there was no need to translate the assembly to cover the field. For the same number of photons detected, the multiple detectors reduced the scan time by a factor of 100 or more. The time to collect information for one slice was less than 10 s. Because a patient could hold his breath for 10 s, it was now possible to take CT images of the chest, but heart motion was a limiting factor in many applications.

The next improvement aligned the third-generation CT machine gantry with several hundred stationary detectors and rotated the x-ray tube. Improvements of the computers, higher output x-ray tubes reduced the scan time to 2 s or less and the slice thickness to around 2 mm. Cables connected the rotating tube to the power supply so that a scan series consisted of a number of winds and unwinds of the cables to make the exposures. For example, the tube would rotate once to make an exposure, the patient table would translate 1 cm, the tube would rotate in the opposite direction while making the next exposure, the table would translate 1 cm, etc. A series of 10 or 15 exposures would permit a study of, say, the liver or abdomen. By using power supplies that rotated with the x-ray tube and by using slip rings to carry power to the assembly, it was not necessary to rotate-reverse-rotate, etc. in order to wind/unwind the x-ray tube cables, and the scan process could proceed with a series of rotate the tube assembly, translate the table, rotate, etc., to complete the exposures for the study.

The most recent improvement is to move the table in a smooth, stepless motion while the tube assembly rotates continuously. This helical or spiral scanning method obtains image data faster than five images/s. Another improvement uses paired detectors so that two cuts 1 cm apart are made simultaneously. These fast image acquisition systems make possible CT angiography of the heart, i.e., dynamic studies of the blood vessels of a beating heart. A practical limitation of any of these systems is the difficulty of rotating a 200 kg mass at several rpm while maintaining precision of the position of the source to within a fraction of a millimeter.

Figure 12.14 shows one novel machine, which avoids the practical problem of accelerating the mass of the x-ray tube and power supplies by building the machine in the form of a “demountable” x-ray tube. Here, the electron beam strikes a circular anode almost 2 m diameter, the patient is within the circle, and the ring of detectors is the same as the fourth-generation machines. Such machines take CT angiographic images faster than 30 images/s.

Figure 12.15 shows that the resolution of the third- and fourth-generation machines can be as high as 512×512 pixels. In some applications, the operator can set the machine to lower values when high resolution is not required and so reduce patient exposure. The early machines used scintillation detectors based on the technology of images for nuclear medicine. In order to pack many detectors into the small space required for high resolution, new detectors were developed. One type uses an “egg crate” assembly of pressurized xenon gas ion chambers. Several hundred cylinder equivalents are arranged in an arc, each feeding an amplifier. The dimensions of each cylinder and the gas pressure are such that the x-ray absorption of the mass of xenon gas along the length of the cylinder is sufficient for detection at reasonable exposure rates (about 10% stopping power). Solid-state detector technology has improved so that small scintillators can be coupled to arrays

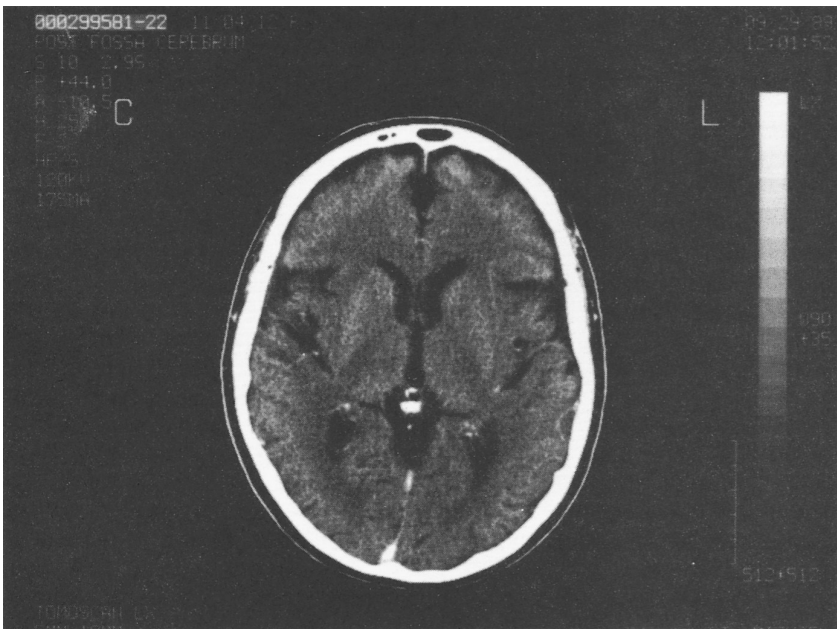


Figure 12.15 A 512 x 512 pixel CT Image of the brain Note that the increased number of pixels yields improved images. (Photo Courtesy of Philips Medical Systems.)

of photodiodes and still have excellent absorption. Newer detectors convert the x radiation directly into electric signals to multiple integrated-circuit amplifiers.

The linear attenuation coefficient of the x-ray beam of the patient tissue can be expressed in dB/cm. However, this term is dependent on beam energy and is often inconvenient to use. Of greater interest to the diagnostician is the relative attenuation corrected for beam energy and other effects. Tissue attenuation can be characterized by values from -1000 H (air) through 0 H (water) to +1000 H (bone). The units are expressed as H units, or Hounsfield units, and are compensated for beam and other effects. Abnormal tissue, bone density, and body fluids are often found by noting deviations of the attenuation in H units.

Figure 12.16 shows that images are presented at the computer console. The operator controls the window width and level (WWL), brightness, and contrast with a wedge showing H units versus gray levels. Patient information and machine settings are also displayed. The patient table moves a preset distance between scans so that several planes or “cuts” can be imaged. The physician can observe the appearance of objects in several different cuts to get an idea of their shape. Computer programs have also been developed that take the information from several cuts and display that information as a



Figure 12.16 Control console and gantry assembly of a CT system (Photo courtesy of Philips Medical Systems.)

three-dimensional image object. For example, the images of cranial bones in several planes can be processed to generate a synthetic image of a complete skull. A duplicate monitor is used in a film camera assembly to photograph the CT images of several cuts and WWLs. Several images are recorded on a single film for the patient record. Physicians often examine CT images at the same time as other type of images, because objects that are obscure in one type of system may be obvious in others.

12.8 MAGNETIC RESONANCE IMAGING

Spinning charged particles have a magnetic moment and, when placed in an external magnetic field, tend to align with the field. The usual state would be for the field of the charged particles to align itself N to S, where N refers to the north pole of the particle's field and S refers to the south pole of the external field. However, it is possible for the particles to be oriented N to N and have the property that a slight perturbation causes the particle to flip back to the lower-energy state, N to S, and thereby return energy to the system. The N-to-N state is a high-energy state; it corresponds to an ionized state (or other excited state) of other particles (Block, 2006).

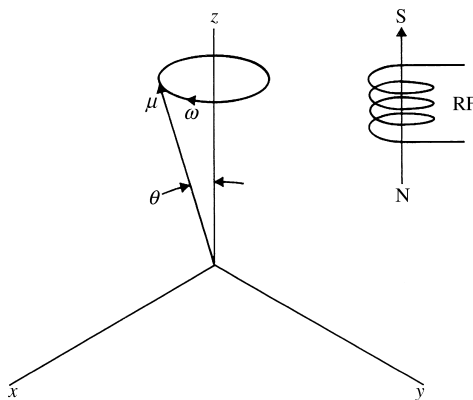


Figure 12.17 Precession of charged particles in a magnetic field.

At any instant, there are particles in the normal state, or rest state, and particles in the excited state. These two states are also called the *spin up* or parallel state and the *spin down* or antiparallel state. The ratio of excited particles to particles at rest is a function of the energy difference between the states and of the temperature. The quantum energy difference is $\Delta E = hf$, where h is Planck's constant and f is the frequency. The ratio of the populations of normal to excited particles is $N_n/N_e = e^{hfkT}$, where k is Boltzmann's constant and T is the temperature. Actually, the axes of the spinning particles do not remain fixed in the magnetic field but rather precess, or wobble just as a spinning top does in a gravitational field (see Figure 12.17). The precessional frequency can be found from the Larmor relationship, $\omega = \gamma B$, where ω is 2π times the precessional frequency, B is the magnetic field, and γ is a property of the particle called the *gyromagnetic ratio*. Resonance—the absorption of energy—occurs when radio-frequency energy is applied at the Larmor frequency and causes particles to change state and become excited.

The particles exist in three-dimensional space, and we can assume that the external magnetic field is along the z axis. Precession also occurs around the z axis. If a pulse of radio-frequency (RF) energy at the precessional or Larmor frequency is applied to the system, the particles absorb energy and the precessional axes rotate. They could rotate just 90° or to the point where they precisely reverse direction of alignment (a full 180°). Because the RF energy and the pulse width determine this angular shift, the pulses are called simply 90° or 180° RF pulses. After the pulse, the particles return to the equilibrium ratio at rates determined by thermal coupling to the lattice and by the exchange of magnetic energy between excited and nonexcited particles. The two types of energy decay are called *spin-lattice decay* (with time constant T_1) and *spin-spin decay* (with time constant T_2). These time constants are quite long, ranging from several milliseconds to seconds, and they depend on the type of particles and the surrounding material. By varying the time between

the RF pulses, their type (90° or 180°), and the placement of receiver coils, it is possible to determine the values of T_1 and T_2 .

The patient axis is the y axis. The patient is placed in the constant magnetic field and then the field is perturbed to produce a small magnetic gradient along the y axis. There will be only one small section or slice at a particular magnetic field value. The surrounding RF coils are then pulsed at the frequency corresponding to the Larmor frequency of the particle being studied, usually the hydrogen nucleus. Because the resonant frequency is sharply defined, only those particles within this slice will be excited. The magnetic field is then quickly perturbed across the patient, along the x axis, and the relaxation decay frequency will vary along the x axis as a function of the magnetic field. The selectivity of the radio receiver will separate signals as if they were scan lines orthogonal to both gradient fields. A more elegant receiver, a spectrum analyzer, produces multichannel signals as functions of frequency to feed to the computer. The magnetic field can be either rotated slightly by introducing perturbations in the z axis or can simply produce a single gradient in the z axis to produce additional sets of scan lines. The similarity to CT systems is obvious, and the multiple line signals are processed in the same way.

Because of the reactance of the large magnetic coils, gradient coils are used to incrementally perturb the field, i.e., produce the small magnetic gradient that is the key to MRI imaging. In addition, magnetic shunts may be used to adjust the primary magnetic field. These produce mechanical noises as they drop in place. The cleverness of the system is impressive: Produce an axial magnetic gradient so that only one plane is excited at the Larmor frequency, then rotate this field (a second gradient coil) to produce and tune the receiver to scan lines across the slice following the exciting pulse of RF energy; rotate the gradient field to scan additional sets of lines; receive the signals in a spectrum analyzer (each channel detects the signal from a single line in the plane); and repeat several hundred times to reduce the noise and process signals as done in CT systems to produce the images.

Because of the time relationships of T_1 and T_2 recovery signals to the initial RF exciting pulse, these may be enhanced by various pulse gate recovery schemes or pulse code systems. By observing the time differences of these signals, the receiver can be gated to accumulate signals of particular time relationships to enhance particular features of the images.

The spinning charged particles could be spinning electrons, either single or unpaired, or charged nuclei—in particular the simplest nucleus, the proton of ionized (in solution) hydrogen. The ratio of excited particles to particles at rest and other properties of particular nuclei determine the sensitivity to nuclear magnetic resonance sensing methods: the nuclear magnetic resonance (NMR) sensitivity. This is a measure of the ease of obtaining useful signals. Table 12.1 characterizes some of the common biological elements.

The nuclear magnetic resonance effects of each of these elements can be measured when a sample is placed in the apparatus with a uniform magnetic field and the excitation frequency is varied. To image a cross section of tissue—in particular, living tissue of a patient—a gradient field is used. For example, if

Table 12.1 Nuclear Magnetic Resonance Frequencies of Common Biological Elements

Element	Percent of Body Weight	Isotope	Relative Sensitivity	NMR Frequency, MHz/T
Hydrogen	10	^1H	1.0	42.57
Carbon	18	^{13}C	1.6×10^{-2}	10.70
Nitrogen	3.4	^{14}N	1.0×10^{-3}	3.08
Sodium	0.18	^{23}Na	9.3×10^{-2}	11.26
Phosphorous	1.2	^{31}P	6.6×10^{-2}	17.24

the field were varied about 1.0 T, the NMR frequency of hydrogen would vary about the 42.57 MHz value tissue section, hydrogen would be present in various densities throughout the sample, and a band of returned frequencies would be detected. Fourier analysis is used to determine the amplitude distribution of the returned frequencies, and one “pass” of the back projection (similar to that of a computerized tomographic image) is determined. Unlike CT, the entire scanner does not have to be rotated; the direction of the magnetic gradient is rotated slightly, and the process is repeated to get the next back projection. The back-projection signals are analyzed by the computer to generate an image of the density distribution of hydrogen in that plane or “cut.” The cut thickness is determined by carefully restricting the field of the RF antenna of the transmitted signal and the return signal. When the NMR signals are used to produce an image in this way, the technique is called *magnetic resonance imaging*.

Unlike CT, MRI uses no ionizing radiation, and no measurable biological after-effects have been seen. Magnetic resonance imaging appears to be safe, so repeated images of delicate tissue can be made without harm or concern for exposure. By varying the sequence code of the 90° or 180° pulse train, the displayed contrast can be intensified for materials of slightly different T_1 and T_2 values.

The magnetic field can be quite strong—on the order of 2.0 T or above. Because most ferromagnetic materials saturate close to that level, superconducting coils are used when very strong fields are required. An alternative is to use either a conventional permanent magnet or a resistive-coil electromagnet when the field is 1.0 T or less. A lower magnetic field means that the Larmor frequency is also reduced and that the lower frequencies degrade the intensity of the received signal and the resolution of the final image. However, resistive-magnet MRI machines are suitable for many imaging applications.

The positioning of the patient in the gantry of the MRI machine is similar to the patient’s positioning in a CT machine. The MRI gantry is deeper to accommodate the magnet over dimensions that will ensure uniformity of the field and to provide RF shielding for the receiving coils. Magnetic

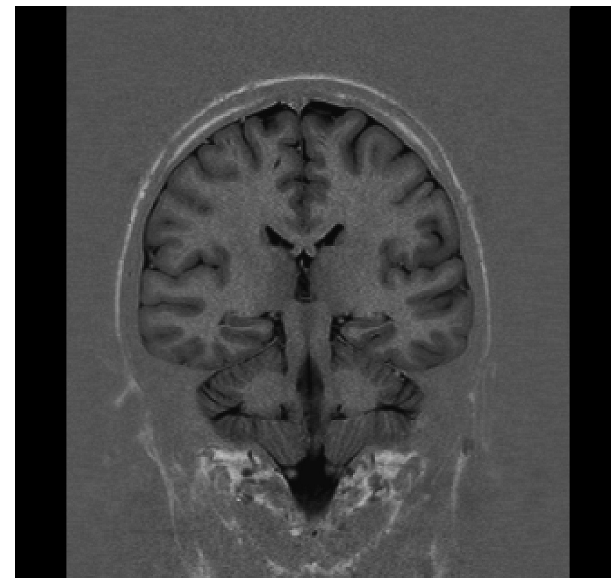


Figure 12.18 MRI image of the head Sets of images may be acquired for 1 mm-section thickness at 2 mm apart for diagnosis of the entire volume of the brain. (Photo courtesy of Siemens Medical.)

resonance imaging scans require up to several minutes, but, as Figure 12.18 and Figure 12.19 show, they are similar in general appearance to the tomographic slices or sections of CT images. Both machines can make a number of slices to determine the level of the anatomical object or anomaly. The diagnostician can examine films of several slices from both CT and MRI machines to obtain the necessary information.

Structural MRI scans display only differences in tissue type. Functional MRI (fMRI) displays changes in blood oxygenation levels. Cognitive activity changes metabolism in regions of the brain, which then increase blood flow and increase oxyhemoglobin, which differs in its magnetic properties from deoxyhemoglobin.

Diffusion-weighted imaging (DWI) uses a pulsed field gradient to measure the diffusion of water to diagnose vascular strokes in the brain. Diffusion tensor imaging (DTI) varies the magnetic field in 6 directions to measure direction of diffusion of water to image white matter tracts in investigations of neural networks.

With dynamic contrast enhanced MRI (DCE-MRI), sites acquire a serial set of images before and after the injection of a paramagnetic contrast agent such as gadolinium. The gadolinium changes the local magnetic field, which changes the Larmor frequency, which changes the contrast. This rapid acquisition of images allows an analysis of the variation of the MR signal intensity, before and after contrast enhancement, over time; recorded for each image

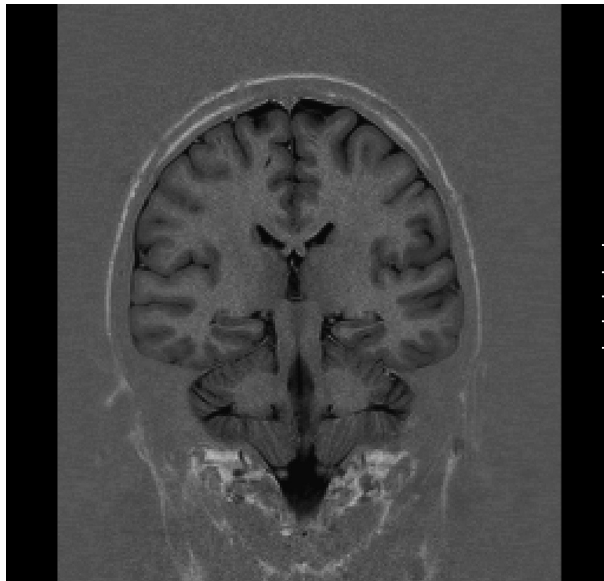


Figure 12.19 MRI image of the brain. Compare with Figure 12.15. The MRI image shows differences due to hydrogen concentration rather than tissue density, making the bony part of the skull transparent and having a different contrast pattern than the CT image. (Image courtesy of Siemens Medical Systems.)

voxel. As the contrast agent enters the tissue, it increases the MR signal intensity from the tissue by a degree that depends on the local concentration. When the contrast agent leaves the tissue, the MR signal intensity decreases toward the baseline value. Using an appropriate pharmacokinetic model, the difference between the two sets of values can be analyzed to determine blood flow, permeability, and tissue volume fractions for each voxel within ROI.

12.9 NUCLEAR MEDICINE

Nuclear medicine enlists radioactive material for the diagnosis of disease and for assessment of the patient. Thus, it differs from radiography in that the source of gamma rays is not external but rather *within* the patient. It also differs in a second very important way: The radioactivity can be attached to materials that are biochemically active in the patient. Therefore, nuclear medicine is said to image *organ function* as opposed to simple organ morphology. The basic imaging situation in nuclear medicine, then, is the measurement of a distribution of radioactivity inside the body of the patient. These distributions can be either static or changing in time (Williams, 2006; Wagner *et al.*, 1995).

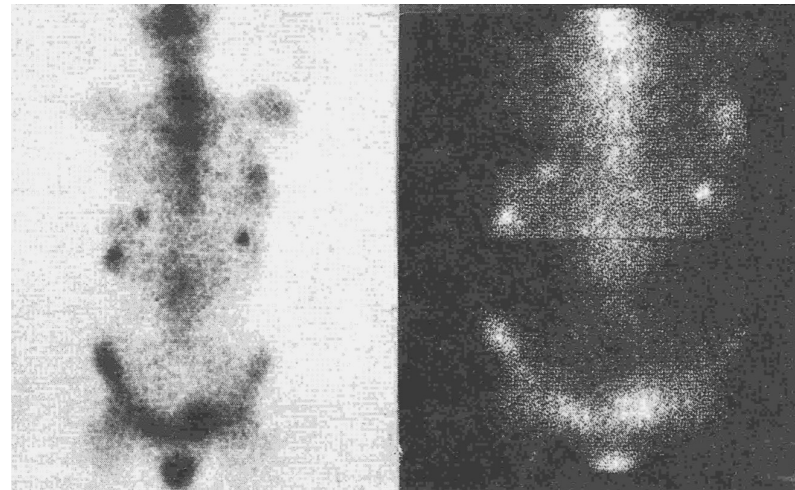


Figure 12.22 Images of a patient's skeleton were obtained by a rectilinear scanner, in which a technetium-labeled phosphate compound reveals regions of abnormally high metabolism. The conventional analog image is on the left, and the digitized version is on the right.

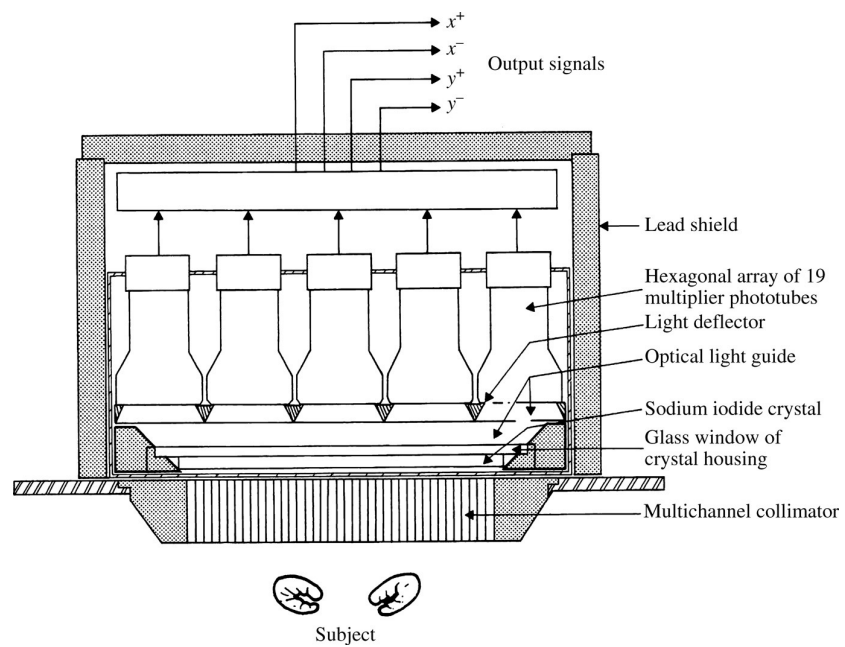


Figure 12.23 Cross-sectional view of a gamma camera (From G. J. Hine, ed., *Instrumentation in Nuclear Medicine*. New York: Academic, 1967.)

Table 12.2 Characteristics of Five Isotopes for PET

Isotope	Maximal Kinetic Energy	Half-life	Broadening
^{10}F	640 keV	110 min	1.1 mm
^{11}C	960 keV	20.4 min	1.9 mm
^{13}N	1.2 MeV	10.0 min	3.0 mm
^{60}Ga	1.9 MeV	62.3 min	5.9 mm
^{82}Rb	3.4 MeV	1.3 min	13.2 mm

12.11 POSITRON EMISSION TOMOGRAPHY

Certain isotopes produce positrons that react with electrons to emit two photons at 511 keV in opposite directions. Positron emission tomography (PET) takes advantage of this property to determine the source of the radiation. If one path is shorter, then the opposite path is longer, and the average signal level is the same without regard to patient attenuation or point of origin. These isotopes have two means of decay, which result in the annihilation of an electron. In one case, the nucleus can capture an orbital electron that combines with one positive charge; alternatively, the nucleus can emit the positive charge as a positron that travels a short distance to combine with an external electron. The combination of the negative and positive particles annihilates the charges and masses of each, energy and momentum are conserved, and two 511 keV gamma rays are emitted in opposite directions.

Positrons emitted by the nucleus have kinetic energy, so they travel a few millimeters before the annihilation emission event. The travel distance and interaction effects blur the dimensions of the region of origin when it is detected. The broadening effect shown in Table 12.2 is the width of the pulse measured at the 10% level. The dimensions of a useful picture element would be about twice these values because of other spreading effects, such as system bandwidth optical effects.

The property of simultaneous emission of two gamma rays in opposite directions gives PET the ability to locate the region of origin. Instead of the multihole collimator found in most gamma cameras, two imaging detectors capable of determining x - y position are used. Each x - y pair is accepted if the two scintillation effects are coincident and have energy levels (pulse heights) close to the expected value of 511 keV.

In the simplest PET camera, two modified Anger cameras are placed on opposite sides of the patient [Figure 12.26(a)]. The modification removes the multihole collimator and adds the coincidence and computing circuits. Removing the collimator increases the collection angle and reduces the collection time, which are limitations of SPECT. The camera is rotated slowly around the patient to obtain the additional views needed for reconstruction and to obtain better images. Images can be built up faster when additional pairs of detectors are used. Figure 12.26(b) shows the three pairs of cameras used in the hexagonal-ring camera. Incremental lateral translation and rotation improve the images by compensating for inhomogeneities and gaps of detection. Very elegant cameras can be constructed by using a circular ring of many detectors that surround the patient [Figure 12.26(c)]. The ring detector does not have to be rotated; image positions are resolved by computer analysis of the signals. As in all radionuclide imagers, the level of the radioactivity places a noise bound on the images. Obviously, compromises must be made in the amount of radionuclide administered: It must be large enough to obtain a good image in the time required and small enough to minimize patient exposure to radiation.

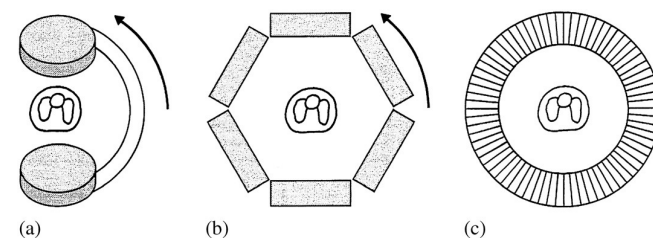


Figure 12.26 Evolution of the circular-ring PET camera (a) The paired and (b) the hexagonal ring cameras rotate around the patient. (c) The circular ring assembly does not rotate but may move slightly—just enough to fill in the gaps between the detectors. The solid-state detectors of the ring camera are integrated with the collimator and are similar in construction to detectors used in CT machines.

The advantages of PET over conventional nuclear imaging include the clarity of the cross-sectional views and the availability of positron emitters that can be compounded as metabolites. It is possible to map metabolic activity in the brain by using tagged compounds to observe uptake and clearance.

The measured quantity in PET imaging is the concentration, in tissue, of the positron emitter. To obtain the actual concentration, it is necessary to calibrate and measure the performance of the machine. Because knowing the actual concentration (in $\mu\text{Ci}/\text{ml}$) in the patient may not be so important as knowing the fraction taken up in a particular region, the PET camera can be used to measure the tissue concentration in arbitrary units. A short time after the imaging procedure, a sample of the patient's blood may be placed in a well counter (a scintillation counter) to obtain a reference value. Comparison of the tissue and blood activity yields the ratio of isotope uptake. For example, the local cerebral blood volume and the distribution of activity are measured this way. Because the brain adjusts uptake as a function of the use of various metabolites, brain activity can be measured. A rapid sequence of brain images shows the response of the brain to various stimuli and pinpoints areas of abnormal activity.

As different parts of the brain respond to different stimuli, the PET image shows this activity (Figure 12.27). Normal brains generate one image of brain activity, but abnormal functioning, tumors, seizure, and other anomalies may also be clearly visible in the map of activity. The PET image of the brain shows the patient's responses to noise, illumination, changes in mental concentration, and other activities. One method of introducing a suitable isotope for brain

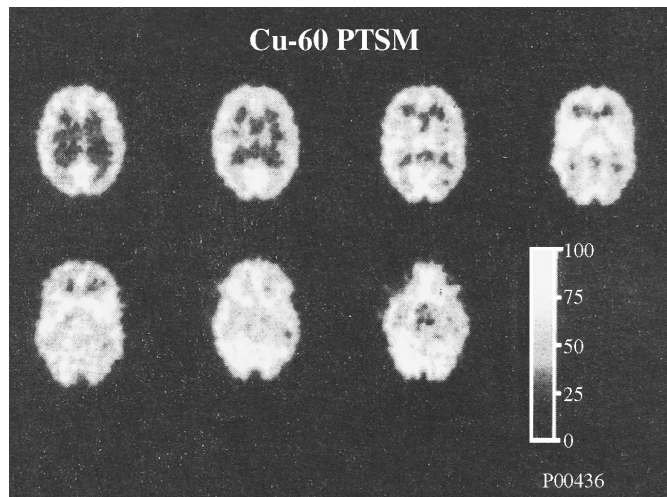


Figure 12.27 PET image The trapping of ^{60}Cu -PTSM (a thiosemicarbazone) reflects regional blood flow, modulated by a nonunity extraction into the tissue. (Photo courtesy of Dr. R. J. Nickles, University of Wisconsin.)

imaging is for the patient to breathe air containing CO made with ^{11}C . Such short-lived positron-emitting isotopes do not occur in nature but can be created in a small cyclotron. This is done by introducing into the nucleus a proton that, in turn, emits an alpha particle or neutron. For certain elements, the nucleus becomes unstable and emits a positron in a short time. For example, ^{11}C is prepared in a small cyclotron and has a half-life of 20.4 min. The short half-life means that the isotope must be prepared near the point of use. The radionuclide decays rapidly, exhibits high activity during the time necessary to obtain images, and clears the patient in a short time. Clearance is a function of both the radioactive decay and the biological excretion of the material.

12.12 ULTRASONOGRAPHY

We know from old war movies that pulses of sound waves are used to detect submarines. Because wavelength λ , frequency f , and velocity u are related ($u = f\lambda$), it is easy to show that wavelengths in the audible spectrum are only a small fraction of the length of a submarine. A phase change of less than one cycle (360°) would result in a maximum error of position equal to the wavelength: $\lambda = u/f$. To find the error of position of a detected submarine, substitute the velocity of sound in water (1480 m/s), and let $f = 1 \text{ kHz}$ and $\lambda = 1.48 \text{ m}$. This precision would be adequate for detecting submarines but not for, say, visualizing a human fetus. To obtain precision of 1.48 mm, the frequency of the pulse would have to be increased to 1.0 MHz in the ultrasonic range.

Sound and ultrasound follow rules of propagation and reflection similar to those that govern electric signals. A transmission line must be terminated in its characteristic impedance to avoid reflections. The acoustic impedance Z is a fundamental property of matter and is related to the density ρ and the velocity of sound u : $Z = \rho u$. The fraction of energy R reflected at the normal interface of two different tissue types is and the impedances are those of the tissues on either side of the interface (Kripfgans, 2006).

$$R = \left(\frac{Z_2 - Z_1}{Z_2 + Z_1} \right)^2$$

Acoustic signals diminish as a function of distance, geometry, and attenuation. In free space, the signals decrease as a result of the inverse square law because the energy per unit area is a function of the total area of the imaginary sphere at distance r . The signals also decrease as a result of attenuation by the medium. When α is the coefficient of attenuation and I_0 is the incident signal intensity, the signal intensity is

$$I = \frac{I_0 e^{-\alpha r}}{r^2}$$

Table 12.3 Acoustic Properties of Some Tissues at 1.0 MHz

Tissue	u , m/s	Z , g/(cm ² ·s)	HVL, cm	R at Interface
Water	1496	1.49×10^5	4100	Air/water
Fat	1476	1.37×10^5	3.8	Water/fat
Muscle	1568	1.66×10^5	2.5	Water/muscle
Brain	1521	1.58×10^5	2.5	Water/brain
Bone	3360	6.20×10^5	0.23	Water/bone
Air	331	4.13	1.1	Tissue/air

When α is large compared to r , the exponential term dominates, and it is convenient to define the thickness of material where the attenuation of the medium decreases the signal by half (the half-value layer or HVL) independently of the geometrical effects. Table 12.3 lists the HVL for water and some tissues. Note that water is not very *lossy* and that the signal decreases 50% for 41 m of water. However, a 50% decrease occurs through only 2.5 cm of muscle. Most biological tissues have high coefficients of attenuation and low HVLs. Attenuation increases with frequency.

Ultrasound transducers use the piezoelectric properties of ceramics such as barium titanate or similar materials. When stressed, these materials produce a voltage across their electrodes. Similarly, when a voltage pulse is applied, the ceramic deforms. If the applied pulse is short, the ceramic element “rings” at its mechanical resonant frequency. With appropriate electronic circuits, the ceramic can be pulsed to transmit a short burst of ultrasonic energy as a miniature loudspeaker and then switched to act as a microphone to receive signals reflected from the interfaces of various tissue types. The gain of the receiver can be varied as a function of time between pulses to compensate for the high attenuation of the tissues. Ultrasonic energy at the levels used for medical imaging appears to cause no harm to tissue, unlike the ionizing radiation of x rays.

The time delay between the transmitted pulse and its echo is a measure of the depth of the tissue interface. Fine structures of tissues (blood vessels, muscle sheaths, and connective tissue) produce extra echoes within “uniform” tissue structures. At each change of tissue type, a reflection results. Figure 12.28 shows how the interfaces of bodily structures produce the echoes that reveal their locations. This type of simple ultrasonic scanner, the A-mode device, was an early device used to measure the displacement of the brain midline. An A-mode device shows echo intensity as an x - y plot. The transducer is placed against the skull and the display gives the echo time of the brain midline (proportional to depth). The transducer is then moved to the other side of the skull and the procedure repeated. The images of normal patients are symmetric so that the brain midline should appear in the same position in the two images. A tumor or large blood clot could move the cerebral hemispheres to shift the midline. This type of simple device is now seldom used and has been

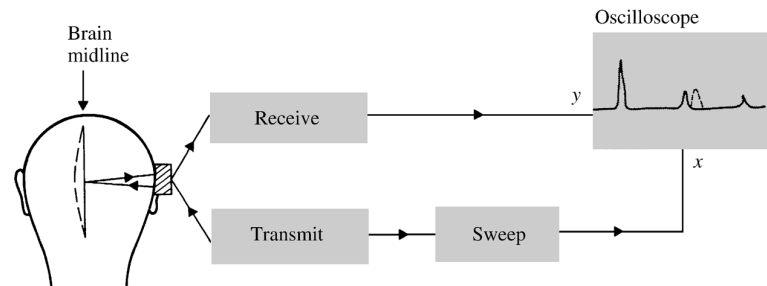


Figure 12.28 A-mode scan of the brain midline.

replaced by more elegant systems that show structures that are far more detailed and also show the brain midline.

EXAMPLE 12.6 For Figure 12.28, estimate the sweep speed required for a 10×10 cm display. Estimate the maximal rate of repetition.

ANSWER For Fig. 12.26, the round trip acoustic distance is about 0.02 m. Acoustic velocity of water is 1500 m/s. Time $t = d/u = 0.02/1500 = 13.3 \mu\text{s}$. Choose a sweep speed of $2 \mu\text{s}/\text{cm}$ or $20 \mu\text{s}$ across the 10 cm display. Maximum repetition rate is $1/(20 \mu\text{s}) = 50 \text{ kHz}$.

If the strength of the echo signal is used to modulate the intensity of the display against the echo-return time, with zero time at the top of the display and with the appropriate image storage circuits, the image can be shown as moving to the right. This technique presents the position of tissues as a function of time as a time-motion (TM) scan. Figure 12.29 shows the motion of the mitral valve of the heart over three cardiac cycles.

Computer image storage displays or long persistence phosphor display screens can be intensity modulated as the position of the transducer is varied. The display will show the two-dimensional shape of objects. For older systems, the position and direction of the transducer are coupled to the display circuits by a system of pulleys and potentiometers. Newer systems use mechanical scanning or phased arrays within the transducer assembly and display the two-dimensional image relative to the fixed position of the transducer assembly. A computer stores the echo signals for display as a sector. Some sophisticated systems correlate sectors taken from a number of directions and display them as a single image, much improved in quality over an image taken from only one direction. Sector images and most two-dimensional images are called *B-mode images* (see Figure 12.30).

Frequencies from 1.0 MHz to 15 MHz are used for most medical ultrasonography. The operating frequency is chosen to meet the imaging task. Higher

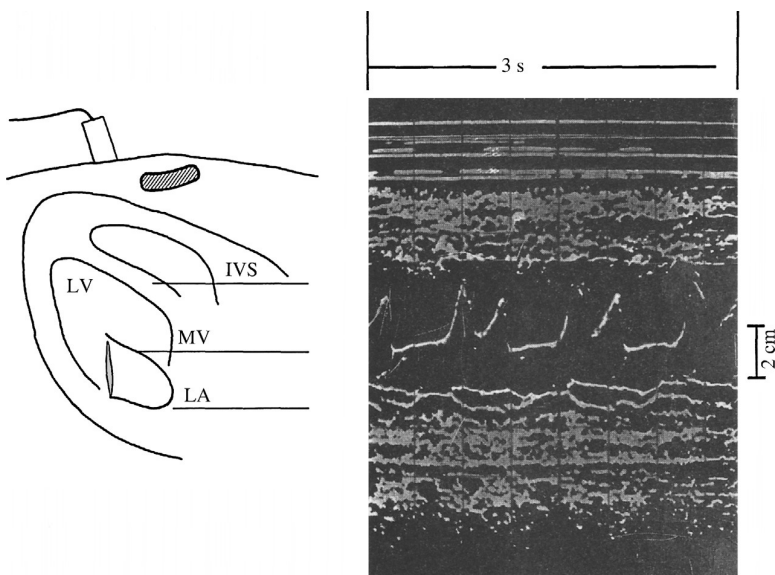


Figure 12.29 Time-motion ultrasound scan of the mitral valve of the heart
The central trace follows the motions of the mitral valve (MV) over a 3 s period, encompassing three cardiac cycles. The other traces correspond to other relatively static structures, such as the interventricular septum (IVS) and the walls of the left atrium (LA).

frequencies will improve resolution, but increased HVL limits the depth of penetration. However, for special purposes (e.g., ophthalmic and neonatal imaging) where the objects are small, the operating frequency may be increased to 15 MHz or higher and the resolution will permit the observation of very small structures or anomalies.

During endobronchial ultrasound (EBUS), a bronchoscope with the ultrasound transducer at the tip is inserted into the windpipe. Images show whether lung cancer has spread into the windpipe or to the lymph nodes on either side.

Figure 12.31 shows four ultrasonic transducers. The two larger devices use three transducers spinning in fluid-filled enclosures [Figure 12.32(a)]. The midsized device and the smaller, ophthalmic transducer use phased arrays, which can be steered by adjusting the timing of the pulses applied to sets of several ceramic elements. If all elements of the transducer are pulsed at the same instant, the ultrasonic energy will be projected in the forward direction [Figure 12.32(b)]. If the left side elements are pulsed in a delayed sequence, the energy will be projected toward the right with the angle proportional to the timing delay [Figure 12.32(d)]. By adjustment of the timing delay, the beam

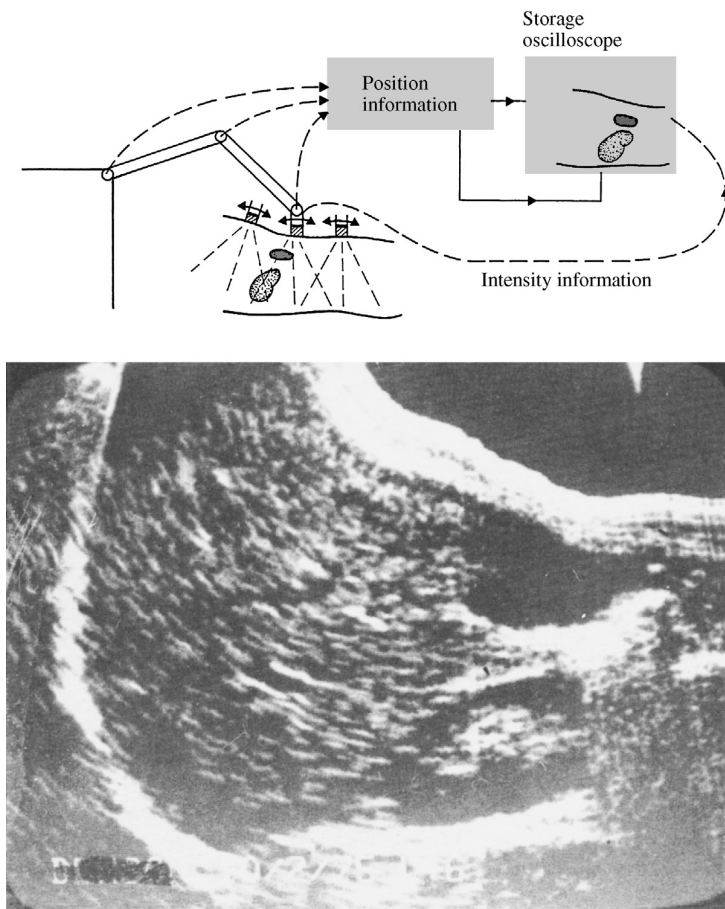


Figure 12.30 (a) B-mode ultrasonic imaging shows the two-dimensional shape and reflectivity of objects by using multiple-scan paths. (b) This B-mode ultrasonic image, which corresponds to (a), shows the skin of the belly at the top right, the liver at the left center, the gall bladder at the right above center, and the kidney at the right below center. The bright areas within the kidney are the collecting ducts.

may be scanned from side to side. With either the spinning or phased array transducer placed against the skin, the image of a sector is displayed. Phased array transducers have been made small enough to be mounted at the ends of probes for insertion into body cavities such as the rectum for imaging the prostate or the vagina for showing the fetus or the condition of the reproductive organs.

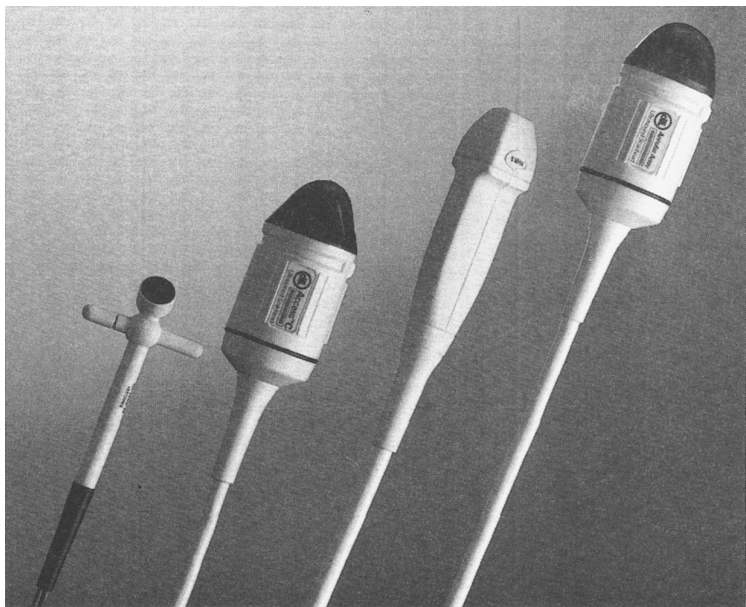


Figure 12.31 Different types of ultrasonic transducers range in frequency from 12 MHz for ophthalmic devices to 4 MHz for transducers equipped with a spinning head. (Photo courtesy of ATL.)

Even smaller transducers have been made for high-frequency operation. These have been fitted at the tips of catheters and used for examining the characteristics of blood vessels prior to angioplasty. Figure 12.33 shows the appearance of a normal artery taken with a catheter tip transducer. In angioplasty, a balloon is introduced into ischemic or partially closed vessels and then inflated to stretch the walls of the vessel to increase the lumen or diameter and increase blood flow. If the vessel walls are weak, the probe images may show that angioplasty could jeopardize the life of the patient. Following balloon inflation, the probe can be pulled back to determine the dimensions of the stretched walls and verify the integrity of the vessel.

DUPLEX SCANNERS

Halberg and Thiele (1986) describe the design of a phased array ultrasonic duplex scanner that combines real-time two-dimensional imaging with the pulsed-Doppler method to measure directional blood velocity noninvasively. Figure 12.32(d) shows how a mechanical real-time sector scanner can generate a fan-shaped beam. Figure 12.34 shows the system block diagram. A colored

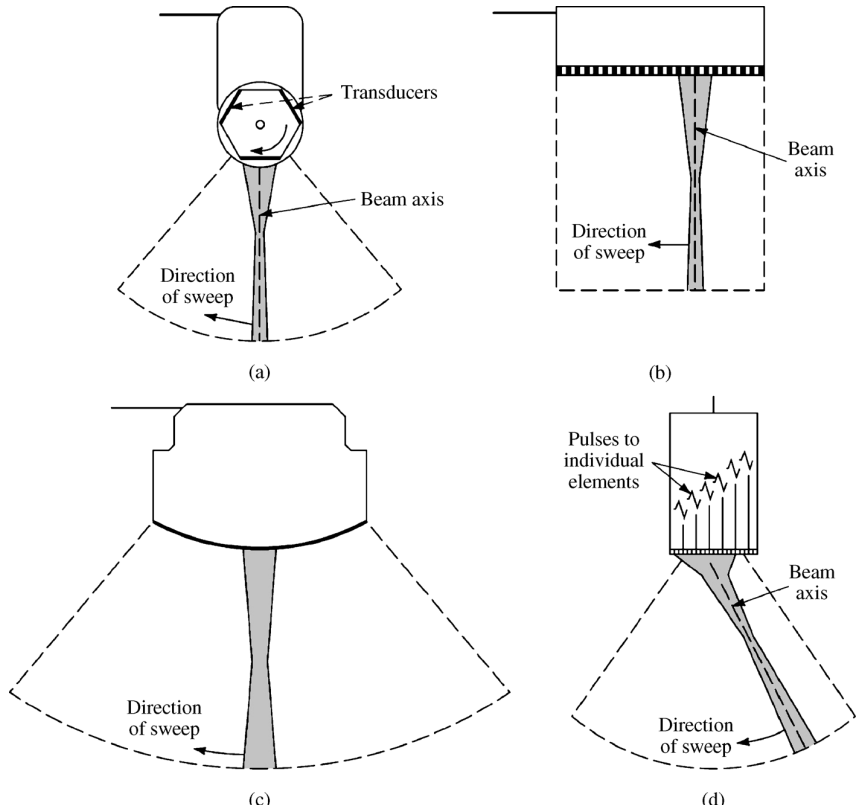


Figure 12.32 Ultrasound scan heads (a) Rotating mechanical device. (b) Linear phased array which scans an area of the same width as the scan head. (c) Curved linear array can sweep a sector. (d) Phasing the excitation of the crystals can steer the beam so that a small transducer can sweep a large area.

display from a duplex scanner shows flow into or out of the screen as red or blue against a monochrome background, with the intensity of the color approximating the velocity. This technique is called *color flow imaging* and yields images shown in Figure 12.35.

Because the duplex scanner can distinguish between moving blood and stationary soft plaque, it is useful for diagnosing obstruction in diseased carotid arteries. Pulsed-Doppler techniques are useful in locating and determining in the heart the direction and extent of abnormal flow, valvular abnormalities, shunt lesions such as patent ductus arteriosus, and ventricular and septal defects.

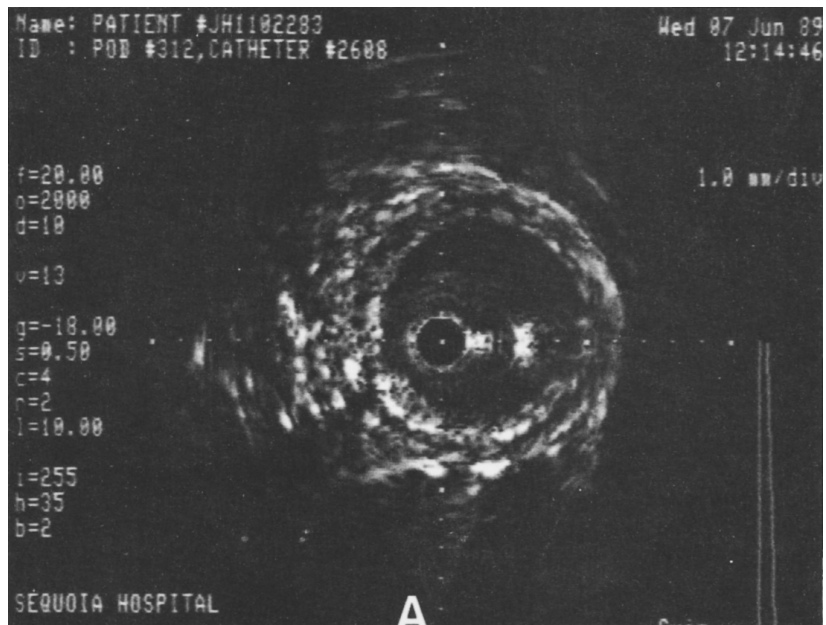


Figure 12.33 Intravascular ultrasonic image showing the characteristic three-layer appearance of a normal artery. Mild plaque and calcification can be observed at 7 o'clock. (Photo courtesy of Cardiovascular Imaging Systems, Inc.)

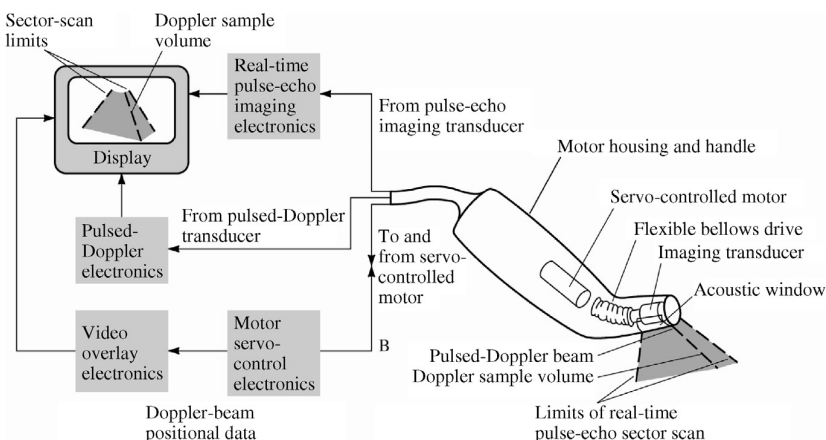


Figure 12.34 The duplex scanner contains a mechanical real-time sector scanner that generates a fan-shaped two-dimensional pulse-echo image. Signals from a selected range along a selected path are processed by pulsed-Doppler electronics to yield blood velocity. [From Wells (1984).]

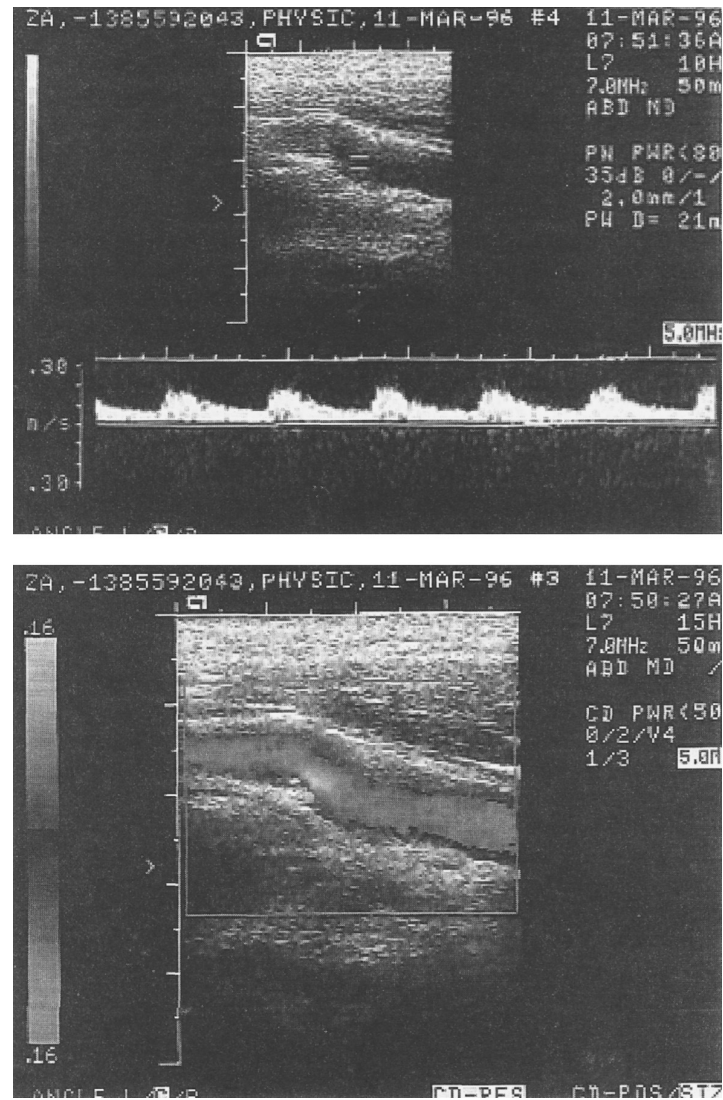
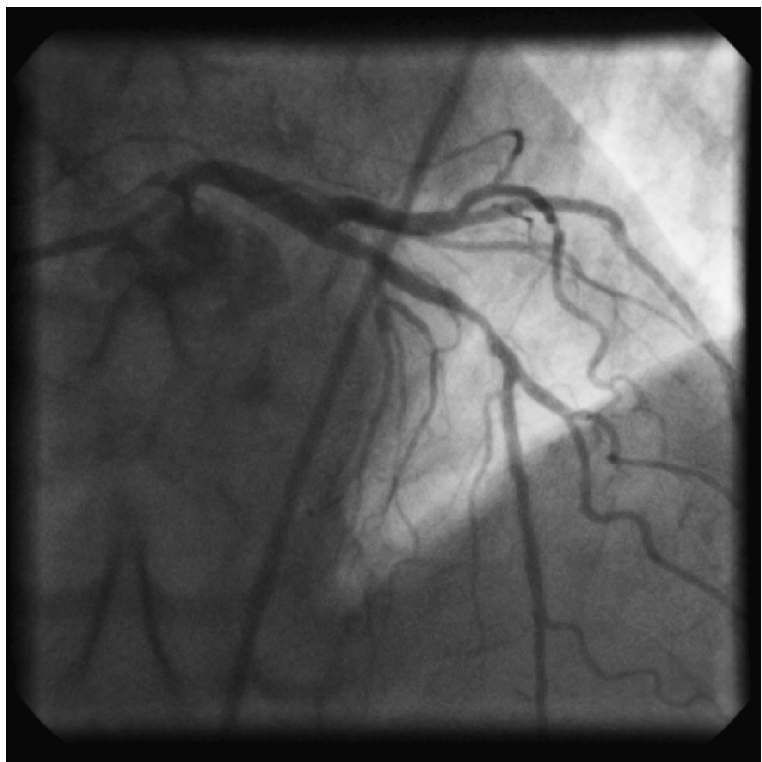


Figure 12.35 (a) Duplex scanner B-mode image and Doppler spectral analysis record for a normal carotid artery, near the bifurcation. The Doppler signals were recorded from the sample volume defined by the Doppler cursor, the two parallel lines located inside the carotid artery. (b) Color flow image of the vessel in (a). Higher velocity components (lighter color, reproduced here in black and white) are seen where the vessel direction courses more directly toward the transducer.

12.13 CONTRAST AGENTS

The images of low contrast structures, blood vessels and anatomic spaces can be enhanced by the injection of a contrast agent. Figure 12.36 shows that for x rays and CT, iodine-based compounds are used as these can be tolerated by the body and expelled quickly. Iodine is a relatively heavy element ($Z = 53$) so that x-ray absorption per atom is high. For MRI, compounds incorporating gadolinium are often used. Gadolinium is unusual in that it is ferromagnetic as a metal and paramagnetic when incorporated in complex organic molecules. Small fat or gas bubbles enclosed in microshells or emulsifiers have different acoustic impedance than most body fluids and will enhance the echo signals.



SIEDBAND,MELVIN
MERITER HOSPITAL LAB 3
202273
12/17/1928
DR. FARNHAM [NEW]

[no scene name]
04/23/2004 8:10:02 AM
LAO: 0.0 CRAN: 40. [Plane A]
Scene: 3

Figure 12.36 Angiogram of the author taken with iodine-based contrast agent. (Image courtesy of Drs. Hinderaker and Farnham.)

The linear attenuation of x rays was given earlier as $I = I_0 e^{-\alpha x}$, where α is the coefficient of attenuation and x is the thickness of the absorber. The mass attenuation coefficient, α/ρ , is found by dividing the linear attenuation coefficient by ρ , the mass of the absorber. The mass attenuation coefficient is roughly proportional to Z^3 , where Z is the atomic number of the absorber. The Z of iodine is 53, and we assume that the average atomic number of blood is less than 5. Iodine contrast agents use complex organic molecules, some having 3 iodine atoms per molecule, usually in the range of 100 to 350 mg/ml. Some iodinated contrast agents are used in angiography and injected into the blood vessels of the heart or other organs to outline the lumens of the blood vessels. Other contrast agents are attached to specialized molecules used as vectors to carry the iodine to, say, the gall bladder or thyroid gland to outline the condition of that organ. As the iodine is expelled by the kidneys, the x-ray image contrast of the urine is increased to permit examination of the ureters, the kidneys, etc. Other iodinated contrast agents increase the contrast of images of the spinal canal and other body cavities, which would otherwise be quite difficult to study.

A ferromagnetic material, such as iron, can show a magnetic field in the absence of an external magnetic field. A paramagnetic material shows a magnetic field in proportion to the external field, the proportion can be greater or less than 1.0. Gadolinium is unusual in that it is ferromagnetic below 22 °C (the Curie temperature) and paramagnetic above it. Since the normal human body temperature is 37 °C, paramagnetic organic molecules can be made that render the high Z (64) element, normally poisonous, tolerable and easy to expel by the kidneys. Because the local magnetic field will be altered by the presence of a paramagnetic substance, the MRI relaxation or decay times, T_1 and T_2 , will also be changed and a high contrast image of the contrast agent will be produced. Such paramagnetic contrast agents can be injected to outline and help visualize lesions in the brain, spine, and associated tissues. Visualization of intracranial lesions due to injuries or tumors is greatly enhanced.

An ideal contrast agent for ultrasound would have impedance quite different from water, blood or nearby tissue in order to increase the visibility of the agent. As in the case for other contrast agents, the material must be well tolerated by the body and readily excreted. Early contrast agents were emulsified oils, which had to be used in high concentrations to be effective. Streams of small air bubbles were not tolerated or the bubbles accreted to form ineffective larger bubbles. The discovery of fullerenes, very large spherical carbon molecules capable of enclosing small volumes, suggested further research and the development of similar microspheres of human albumin enclosing a minuscule volume of air. Further work substituted octafluoropropane gas for the air. The fluorine compound is less soluble in water so that the useful lifetime of the albumin-microsphere-octafluoropropane is several minutes. Such contrast agents, also called *gas microbubbles*, injected into the bloodstream permit the ready visualization of heart structures not easily seen

without the contrast agent such as the coronary valves, the apex, and the shape of the ejected fraction of the blood.